Title: Asymmetric effective connectivity within frontoparietal motor network underlying motor imagery and motor execution

Author:

Takeshi Ogawa[a], Hideki Shimobayashi[a,b], Jun-ichiro Hirayama[c,d], Motoaki Kawanabe[a,d]

Affiliation:

[a]Cognitive Mechanisms Laboratories, Advanced Telecommunications Research Institute International

2-2-2 Hikaridai, Seika-cho, Soraku-gun, Kyoto, 618-0288, Japan

[b]Graduate School of Information Science and Technology, The University of Tokyo

7-3-1 Hongo, Bunkyo-ku, Tokyo 113-8656, Japan

[c]Human Informatics and Interaction Research Institute, National Institute of Advanced Industrial Science and Technology (AIST)

[d]RIKEN Center for Advanced Intelligence Project

2-2-2 Hikaridai, Seika-cho, Soraku-gun, Kyoto, 618-0288, Japan

Takeshi Ogawa: t.ogawa@atr.jp.

Hideki Shimobayashi: shimobayashi@star.rcast.u-tokyo.ac.jp.

Abbreviations: L/R-ME: motor execution with left/right hand; L/R-MI: motor imagery with left/right hand; L/R-FMG: left/right frontomarginal gyrus; L/R-DLPFC: left/right dorsolateral prefrontal cortex; L/R-vPMC: left/right ventral premotor cortex; L/R-dPMC: left/right dorsal premotor cortex; L/R-M1: left/right primary motor cortex; L/R-SPL: left/right superior parietal lobule; L/R-IPS: left/right inferior parietal sulcus; L/R-IPL: left/right inferior parietal lobule; L/R-A1: left/right primary auditory cortex; CS: cue stimulus; DAG: directed acyclic graph; DCM: dynamic causal modeling; EPI: echo planar image; GCM: granger causality mapping; ICA: independent component analysis; IS: instruction stimulus; LiNGAM: linear non-Gaussian acyclic causal model; PCA: principle component analysis; ROI: regions of interest; SMA: supplementary motor area;

Jun-ichiro Hirayama: junichiro.hirayama@aist.go.jp
Motoaki Kawanabe: kawanabe@atr.jp

Corresponding Author:
Takeshi Ogawa, Ph. D
2-2-2 Hikaridai, Seika-cho, Soraku-gun, Kyoto, 618-0288, Japan
TEL: +81-774-95-1413
FAX: +81-774-95-1236
E-mail: t.ogawa@atr.jp

Abstract:

Both imagery and execution of motor controls consist of interactions within a neuronal network, including frontal motor-related regions and posterior parietal regions. To reveal neural representation in the frontoparietal motor network, several approaches have been proposed: one is decoding of actions/modes related to motor control from the spatial pattern of brain activity; another is to estimate effective connectivity, which means a directed association between two brain regions within motor regions. However, a motor network consisting of multiple brain regions has not been investigated to illustrate network representation depending on motor imagery (MI) or motor execution (ME). Here, we attempted to differentiate the frontoparietal motor-related networks based on the effective connectivity in the MI and ME conditions. We developed a delayed sequential movement and imagery (dSMI) task to evoke brain activity associated with data under ME and MI in functional magnetic resonance imaging (fMRI) scanning. We applied a linear non-Gaussian acyclic causal model to identify effective connectivity among the frontoparietal motor-related brain regions for each condition. We demonstrated higher effective connectivity from the contralateral dorsal premotor cortex (dPMC) to the primary motor cortex (M1) in ME than in MI. We mainly identified significant direct effects of dPMC and ventral premotor cortex (vPMC) to the parietal regions. In particular, connectivity from the dPMC to the superior parietal lobule (SPL) in the same hemisphere showed significant positive effects across all conditions. Instead, interlateral connectivities from vPMC to SPL showed significantly negative

effects across all conditions. Finally, we found positive effects from A1 to M1 in the same hemisphere, such as the audio motor pathway. These results indicated that sources of motor command originated from d/vPMC and influenced M1 as achievements of ME and MI, and the parietal regions as integration of somatosensory and visual representation during finger tapping. In addition, sequential sounds may functionally facilitate temporal motor processes.

Keywords:

Motor imagery, finger tapping, fMRI, causal discovery, frontoparietal network

1. Introduction

Achievements of motor imagery (MI) and motor execution (ME) consist of interactions within a neuronal network, including frontal motor regions and posterior parietal regions. According to previous studies, MI is defined as a mental simulation or a mental rehearsal of movements without any overt physical movements (Hanakawa et al., 2008; Lorey et al., 2014; Pilgramm et al., 2016). Neural activities during MI can be predominantly modulated by tasks containing visual, auditory, and kinesthetic aspects (Hanakawa, 2016). Neural substrates of the motor system have common and specific representations corresponding to MI or ME.

Previous studies have reported that information associated with MI can be extracted from activation patterns represented in the frontoparietal network (Apšvalka et al., 2018; Gallivan et al., 2011, 2013; Gao et al., 2011; Hanakawa et al., 2008; Kasess et al., 2008; Lorey et al., 2014; Nambu et al., 2015; Pilgramm et al., 2016; Yokoi & Diedrichsen, 2019; Zabicki et al., 2017). Anatomical brain regions in the frontoparietal network were associated with the following motor processes: i) the primary motor cortex (M1) and primary somatosensory cortex (S1) are activated during the sequential movement; ii) the dorsal premotor cortex (dPMC), ventral premotor cortex (vPMC), and supplementary motor area (SMA) are activated during the preparation period of the movement (Hanakawa et al., 2008; Nambu et al., 2015); iii) neural activation in parietal regions, including the inferior parietal sulcus (IPS), inferior parietal

lobule (IPL), and superior parietal lobule (SPL) have represented gestures (Pilgramm et al., 2016; Zabicki et al., 2017) and target locations depending on head- or eye-centered coordinates and arm/limb-centered coordinates (Gallivan et al., 2011). These findings suggest that achievements of MI and ME consist of interactive communication between brain regions in the frontoparietal network.

To evaluate the functional relationship between multiple brain regions associated with MI and ME, it is important to investigate the effective connectivity of the frontoparietal network, including both hemispheres (Hanakawa, 2016). Previously, several studies identified the effective connectivity of the ME and MI, such as the relationship between SMA and M1 using dynamic causal modeling (DCM) (Kasess et al., 2008; Penny et al., 2004) and a frontoparietal network using Granger causality mapping (GCM) (Deshpande et al., 2008; Gao et al., 2011). DCM is one of the approaches to estimate effective connectivity based on a neurophysiological model. However, selecting the best model (i.e. connectivity pattern) from all possible ones is often infeasible in DCM, especially, given many brain regions and related factors of interest (Smith et al., 2011). GCM is a data-driven method and can be more efficient than DCM. A variant conditional GCM (Ding et al., 2006) was applied to analyzing fMRI data of ME/MI conditions (Gao et al., 2011), demonstrating an asymmetry of effective connectivity in right handedness. However, (conditional) GCM for many brain regions is also not very straightforward as it typically needs to evaluate the Granger causality measure separately for every single

connection.

Asymmetry between the contralateral and ipsilateral regions in the frontoparietal network is a characteristic aspect of motor-related processing that arises depending on handedness. In general, M1 in both hemispheres is activated during MI and ME, but the region contralateral to a controlled hand shows relatively higher activity than the ipsilateral region because of inhibition from the contralateral M1 to the one ipsilateral to the hand in adults (Hanakawa et al., 2005). Ipsilateral M1, however, also encodes single finger movements during ME, even though the mean activation is lower as revealed by a decoding analysis (Diedrichsen et al., 2013). The asymmetric properties of motor control can appear not only in the mean activation or decoding accuracies, but also in effective connectivity. In fact, Gao et al., using conditional GCM, have reported that bidirectional effective connectivities were extracted in the left-hand task, in particular, among L-SPL, L-IPL and L-dPMC (Gao et al., 2011). However, asymmetric network structures of the many known motor-associated regions in the frontoparietal network and related networks, in particular with both hemispheres, have been poorly understood.

Here, we investigated the effective connectivity of the frontoparietal and related networks during MI and ME. In order to apply a data-driven approach and machine learning method, we developed a delayed sequential movement and imagery (dSMI) task extended from a task proposed by Hanakawa et al. (2008)

to acquire enough fMRI data samples under ME and MI (Hanakawa et al., 2008). We newly applied DirectLiNGAM (Shimizu et al., 2011), an algorithm to estimate a linear non-Gaussian acyclic causal model (LiNGAM: Shimizu et al., 2006), to the fMRI time courses in the motor-related regions of interest (ROIs), and estimated their effective connectivity for each condition. DirectLiNGAM is particularly suitable to analyzing large-scale connectivity structures with many ROIs, as compared to DCM/GCM. Finally, we statistically evaluated the effective connectivity within frontal regions, between frontoparietal regions, and between audio motor regions.

2. Methods

2.1 Participants

A total of 27 adults (3 female, mean age = 25.4 ± 5.9 years) participated in this study. Participants received cash remuneration for their involvement in this experiment. All participants had normal or corrected-to-normal vision, no reported history of drugs that affected the central nervous system, and no neurological disease. All participants provided written informed consent prior to the experiment. All participants were right-handed, as assessed by the Edinburgh Handedness Inventory (Oldfield, 1971). This study was approved by the ethical committee of the Advanced Telecommunications Research Institute International (ATR) and followed the Declaration of Helsinki.

2.2 Delayed sequential movement and imagery task

We conducted a dSMI task, which was modified from the original version (Hanakawa et al., 2008) because we needed to collect enough trials within a limited fMRI experiment time. Because of our modification, we collected data samples to apply for the prediction of hands/modes using the machine learning method and optimize the effective connectivity with a data-driven approach. We wrote an in-house program coded for the dSMI task using Psychophysics Toolbox extensions (Brainard, 1997; Kleiner et al., 2007; Pelli, 1997) in MATLAB (MathWorks Inc., Natick, USA). In brief, each run incorporated both performance modes (MOVE: movement; IMAGE: imagery; LISTEN: listening) in a pseudorandom manner. Three different classes of visual stimuli were alternately presented (Fig. 1). An instruction stimulus (IS) was an Arabic numeral semi-randomly selected and visually presented among 1, 2, and 3 for 2 s corresponding to the initial finger, such as the pointing finger, middle finger, and ring finger, respectively. After the IS, a cue stimulus (CS) was presented for 2 s. The CS was one of three visual word stimuli, MOVE, IMAGE, and LISTEN. Each participant was instructed to sequentially tap following short beep sounds (MOVE or IMAGE) or passively listening to the beep sounds (LISTEN) in one of the modes, movement, imagery, and listening, respectively. The participants were required to press the response buttons corresponding to the beep sound (duration = 0.2 s; tone = 500 Hz; frequency = 0.667 Hz) following the instructed sequence in response to the MOVE stimulus (MOVE trials) during D1 period, and press the response button corresponding to the next finger. In response to

the IMAGE stimulus, the participants were asked to image the finger tapping during D1 (7 s) from the instructed finger as performed by him/her (first-person perspective) without actual finger tapping (IMAGE trials), and then, were required to press the response button that corresponds to the next finger. In the case of LISTEN, the participants were asked to respond not only without movement of their fingers but also without imagining their finger movements during the D1 and Answer periods. The MOVE, IMAGE, and LISTEN stimuli were pseudo-randomly assigned to the cue stimuli; therefore, the participants were unable to predict the forthcoming performance mode. The interstimulus interval (ISI) pseudo-randomly lasted for 8, 10, or 12 s. Finally, we corrected 30 trials in four conditions (right ME: R-ME; right MI: R-MI; left motor execution: L-ME; left motor imagery: L-MI). We did not compare the LISTEN condition in further analysis.

2.3 MRI data acquisition

Images were acquired with 3T MRI scanners, MAGNETOM Trio Tim (Siemens Medical Systems, Erlangen, Germany) installed in the Brain Activity Imaging Center in the ATR. High-resolution T1-weighted structural images were acquired for normalization to a standard brain for echo planar image (EPI) registration purposes (TR = 2300 ms, TE = 2.98 ms, flip angle = 9°, TI = 900 ms, matrix = 256 × 256, field of view = 256 mm, slice thickness = 1 mm, iso-voxel). Functional images were acquired with an EPI sequence (TR = 2000 ms, TE = 30 ms, flip angle = 80°, matrix = 64 × 64, field of view = 212 mm, slice thickness

= 3.2 mm, gap: 0.8 mm, 33 slices, scan sequences: interleaved) of 536 volumes in the dSMI task for 17 min 52 s.

2.4 Data analysis

2.4.1 Preprocessing of fMRI data

We followed a preprocessing protocol from a previous study (Ogawa et al., 2018). The data were processed using SPM12 (Wellcome Trust Centre for Neuroimaging). The first four volumes were discarded to allow for T1 equilibration. The remaining data were corrected for slice timing and realigned to the mean image of that sequence to compensate for head motion. Next, the structural image was co-registered to the mean functional image and segmented into three tissue classes in the MNI space. Using associated parameters, the functional images were normalized and resampled in a 2 × 2 × 2 mm grid. Finally, they were spatially smoothed using an isotropic Gaussian kernel of 8 mm full-width at half maximum.

2.4.2 Regions of interest

We followed a previous study (Zabicki et al., 2017) to mostly choose 16 brain regions and added bilateral dorsolateral prefrontal cortex (DLPFC) as control. Therefore, we defined 18 ROIs (Table 1) as follows : frontal motor regions (M1, dPMC, vPMC), posterior parietal regions (SPL, IPL, IPS), and unrelated regions (primary auditory cortex: A1, fronto-marginal gyrus: FMG, dorsolateral prefrontal cortex: DLPFC). The anatomical masks were reconstructed from the Destrieux

Atlas (Destrieux et al., 2010) in the Wake Forest University Pick Atlas (Maldjian et al., 2003). These masks were resliced to match the preprocessed EPIs with the same spatial resolution.

For each participant, we extracted fMRI time courses within each ROI. To remove several sources of spurious variance along with their temporal derivatives, linear regression was performed, including six motion parameters in addition to averaged signals over gray matter, white matter, and cerebrospinal fluid. Furthermore, to reduce spurious changes caused by head motion, the data were checked by a method that reduces motion-related artifacts. A band-pass filter (transmission range, 0.008−0.1 Hz) was applied to these sets of time courses prior to the following regression procedure. Eleven participants were excluded from the fMRI analysis because the participants did not perform all sessions of the experiment or moved head/body too much during fMRI scans.

2.4.3 DirectLiNGAM

Linear non-Gaussian acyclic causal model (LiNGAM: Shimizu et al., 2006) is a causal discovery model that utilizes higher-order distributional statistics to determine directed network connections. The assumption of LiNGAM is that 1) each node (variable) is linearly related to the other nodes, 2) its residual or external input has non-Gaussian distributions, and 3) corresponding directed dependency graph is acyclic, i.e., the nodes have a natural ordering. Letting x_i denote the i-th observation variable, we write its linear association to preceding/parent variable as

$$x_i = \sum_{k(j)<k(i)} b_{ij} x_j + e_i \quad (1)$$

where b_{ij} is the connection weight, quantifying the direct causal effect, and $k(i)$ is the causal order for each variable. The external influences e_i have non-Gaussian distributions, with non-zero variances, and are independent of each other. Rearranging equation (1) into a matrix form, we have

$$\mathbf{x} = \mathbf{B}\mathrm{x} + \mathbf{e} \quad (2)$$

where $\mathbf{x}$ and $\mathbf{e}$ are the vectors of observed variables $\mathrm{x_i}$ and external influences e_i, respectively; $\mathbf{B} = (b_{ij})$ is an $m \times m$ connectivity matrix that can be permuted to a strictly lower triangular matrix (i.e. with all zeros in the main diagonals as well as the upper triangular part). Then, the identifiability of matrix $\mathbf{B}$ and thus the causal ordering/strength among the variables can be rigorously proven (Shimizu et al., 2006) based on the theory of independent component analysis (ICA) (Hyvarinen et al., 2001).

We specifically used DirectLiNGAM algorithm to estimate the strength of effective connectivity (i.e. nonzero entries of B) among brain regions for each of the MI/ME conditions. DirectLiNGAM requires no algorithmic parameters and is guaranteed to converge to an accurate solution within a small fixed number of steps if the data strictly follows the assumptions with sufficiently large samples. During the optimization process, the algorithm also prunes redundant edges and selects significant edges in an acyclic manner. This is important to concisely visualize the directed acyclic graph (DAG) with multiple ROIs and interpret differences across conditions. We used an open-source MATLAB

implementation of DirectLiNGAM (Shimizu et al., 2011).

We first prepared a matrix of time courses of fMRI signal that extracted six data sample epochs from the onset of the D1 period for each ROI (number of voxels × 900 samples; ME and MI conditions contained 30 trials, and the passive listening condition (PL) contained 15 trials, 6 samples × (30 trials × 4 conditions + 15 trials × 2 conditions) = 900 samples; Fig.2A). After normalizing the matrix by the mean and variance of the matrix, we conducted principle component analysis (PCA) for each ROI to decompose the loadings and scores (Fig. 2B). We corrected the sign of the first principal component (PC1) so that it has a positive correlation with the mean time course within the ROI. We collected the corrected PC1 across all ROIs and concatenated the matrix across all subjects for each condition (ME, MI: 18 ROIs × 2,880 samples (6 samples × 30 trials × 16 subjects), Fig. 2C). We applied DirectLiNGAM for each condition, and estimated the $\mathbf{B}$ matrix, the nonzero entries of which identify the direct causal effects, i.e. effective connectivity, between two nodes, as well as the acyclic causal ordering of the nodes.

2.4.4 Statistics of network strength with bootstrapping

To statistically compare effective connectivity**,** such as the direct effect, we applied the bootstrapping method to estimate the lower and upper boundary of the strength of the connections. We resampled the data matrix $\mathbf{x}$ by trial for each condition and estimated the $\mathbf{B}$ matrix with 1,000 repetitions. Finally, we

obtained 1,000 models of DirectLiNGAM and the distribution of strength of a single connection for each condition and confirmed that a confidence interval of 95% is larger than 0.

3. Results

3.1 Effective connectivity on fMRI data

Applying the DirectLiNGAM algorithm, we estimated the weight coefficient matrices, $\mathbf{B}$, from data $\mathbf{x}$ for each condition (R-ME, R-MI, R-PL, L-ME, L-MI, L-PL). By applying the bootstrapping method for each condition, we extracted significant edges with 1,000 repetitions (Fig. 3). To compare effective connectivity across conditions, we focused on three networks: i) motor network (from d/vPMC to M1), ii) frontoparietal network (from d/vPMC to SPL/IPS/IPL), and iii) audiomotor network (from A1 to M1).

First, we determined the motor network, which is the most dominant and essential connection to achieve motor command in the contralateral hemisphere (orange dotted boxes in Fig. 3E-H). We found positive direct effects from dPMC to M1 in the same hemisphere contralateral to the hand (L-dPMC → L-M1, R-dPMC → R-M1) across all conditions. We also identified positive direct effects from dPMC to M1 in the ipsilateral hemisphere. On the other hand, we found negative direct effects from L-dPMC to R-M1 across all conditions. The positive direct effects in the same hemisphere showed symmetric structure, however, the interhemispheric effective connectivity with negative effects showed

asymmetric structure. Connectivity from vPMC to M1 did not show consistency between modes or hands. Thus, the primary motor process might require causal effects from dPMC to M1 to achieve ME and MI.

Second, we focused on the frontoparietal network, in particular, from d/vPMC to SPL/IPS/IPL (blue dotted boxes in Fig. 3E-H). In all conditions, we commonly found positive direct effects from L-dPMC to L-SPL, R-dPMC to R-SPL, L-dPMC to L-IPS, and negative direct effects from L-vPMC to R-SPL, R-vPMC to L-SPL. Meanwhile, connectivity from the parietal regions to frontal regions had not been selected by DirectLiNGAM.

Surprisingly, we found a significant effect from A1 to M1 in the same hemisphere because we added A1 into our analysis as control regions to represent motor processes associated with MI and ME. In particular, strong direct effects were estimated in the condition of the hemisphere contralateral to the executive or imagery hand. Furthermore, we could not find significant direct effects from any region of interest to A1. This suggests that A1 might not be influenced by other regions to achieve the dSMI task, but A1 has an influence on M1. In the dSMI task, we used a sequential pitch to lead finger tapping smoothly for the participants.

3.2 Differences of direct effects due to modes and laterality

To evaluate the direct effects between the two conditions, we evaluated

differences between two samples (A: L-ME vs. L-MI, B: R-ME vs. R-MI, C: L-ME vs. R-ME, and D:L-ME vs. L-MI in Fig. 4) obtained by the bootstrapping method. We compared elements that showed direct effects between two regions in both conditions, and selected nodes that contained differences between two conditions (a confidence interval is more than 0). Obvious differences in effective connectivity are represented in the edges from dPMC to M1 and from A1 to M1, contralateral to the hand (Fig. 4 A and B). The direct effects from dPMC to M1 are more strongly affected in ME than in MI. This edge is essential to achieve motor control and related imagery. Second, the strength of the edges from A1 to M1 is also higher in ME and MI. It may represent a clear neural representation in both regions in the case of ME. In addition, we found asymmetric properties of the edge from L-A1 to L-M1, R-vPMC to R-IPL from R-M1 to L-FMG, and from L-M1 to R-IPL.

Comparing the laterality of ME (Fig. 4C) and MI (Fig. 4D), the edges from dPMC to M1 in the contralateral to the hand clearly show differences in laterality. In comparison to ME, we identified edges from L-M1 to R-IPL, from R-dPMC to R-IPS larger in R-ME, and edges from R-IPS to R-IPL in L-ME (Fig. 4C). In the case of MI, we identified edges from L-M1 to L-SPL, R-M1 to L-FMG, R-IPL to R-DLPFC larger in R-MI, and edges from L-IPL to L-DLPFC, from R-A1 to R-M1 (Fig. 4D).

4. Discussion

In this study, we attempted to distinguish direct acyclic graphs representing the frontoparietal motor network underlying ME and MI. In applying DirectLiNGAM to the fMRI data, we estimated the effective connectivity of multiple brain regions involved in both ME and MI conditions in a data-driven manner. We demonstrated higher effective connectivity from the contralateral dPMC to M1 in ME than in MI. Second, we mainly identified significant direct effects from d/vPMC to parietal regions, including the SPL, IPS, and IPL. In particular, connectivity from the dPMC to SPL in the same hemisphere showed significant positive effects across all conditions. Instead, interlateral connectivities from vPMC to SPL showed significantly negative effects across all conditions. Third, we found positive effects from A1 to M1 in the same hemisphere. Finally, our results of DirectLiNGAM did not select effective connections from the parietal regions to the frontal motor regions. Here, we would like to discuss not only the differences between ME and MI, but also effective connections including motor, frontoparietal, and audiomotor networks.

4.1 Contra-/ipsi-lateral effective connection in the primary motor area underlying ME and MI

We demonstrated strong positive direct effects from dPMC to M1 in the same hemisphere contralateral to the tapping hand during MI and ME (Fig. 3). Previously, positive effective connectivity has been found from dPMC/SMA to M1 (Gao et al., 2011; Kasess et al., 2008; Zhuang et al., 2005). Gao et al.

demonstrated that both the effective connectivity networks and the In-Out degrees, which show information flow consistently left lateralization for right-handed subjects using GCM. With R-ME and R-MI tasks, significant effective connectivity was found between L-dPMC and L-M1 (Gao et al., 2011). Using another approach such as DCM, the results also supported the effective connectivity between L-SMA and L-M1 during the R-ME and R-MI tasks, and identified that a model has a strong suppressive influence on the MI condition (Kasess et al., 2008). One of the reasons for the higher activations observed in contralateral motor areas is that the contralateral M1 inhibits ipsilateral M1 after normal development in adults (Hanakawa et al., 2005). In childhood, neural activity from a single hand reaches M1 in both hemispheres. It supports the ipsilateral activities observed in the ipsilateral hemisphere. We found negative connectivity from L-dPMC to R-M1 in all conditions, but not the opposite side. Our results also show consistency of effective connectivity from dPMC to M1, despite different types of algorithms. This may be a reliable benchmark to evaluate DirectLiNGAM by applying it to our fMRI data.

During MI, less effective connectivity was found compared to that during ME, implying weaker transmission of information among activated brain regions during MI. However, contralateral lateralization still existed. Since MI is associated with motor preparation, anticipation, restraint, execution, and learning (Gao et al., 2011; Hanakawa et al., 2008; Nambu et al., 2015), some common neural representations can be anticipated between ME and MI along

with similar contra-lateralized expressions in causal networks. The role of dPMC contralateral to the tapping hand is encoded by motor planning/preparation (Hanakawa et al., 2008; Nambu et al., 2015). During the preparation period, spatial patterns of brain activities in dPMC and SMA were key contributions to the classification of two sequential movements. In addition, they found that parietal regions including L-SPL, L-IPS and L-IPL, and R-dPMC and M1 during execution were able to classify the two temporary well-organized sequences of movements represented as a set in the brain (Nambu et al., 2015). Furthermore, Hanakawa et al. demonstrated that the time courses of fMRI signals in L-M1 were delayed from those in L-dPMC. In their results, the first peak of fMRI signal changes appeared before the onset of ME and MI in L-dPMC, L-SMA, and L-vPMC. After that, the fMRI signal was increased in M1 in the case of ME, but not in MI (Hanakawa et al., 2008). Our results of direct effects from dPMC to M1 contralateral to the tapping hand robustly show the process from motor planning/preparation to execution of ME and MI with a data-driven approach. It seems that the neural representations of the preparation are generated in dPMC and transferred to M1 to execute not only ME but also MI.

We evaluated prediction models to classify modes/hands from neural representations using MVPA (Supplementary Fig. 1). Classification accuracies of L-MI vs. R-MI in M1 were lower than those of L-ME vs. R-ME in M1. According to previous findings, the effective connection from dPMC to M1 is dominant to achieve small elements of movement based on the generated

motor preparation/plan in dPMC (Nambu et al., 2015; Yokoi et al., 2018; Zabicki et al., 2017). To distinguish hand actions using MVPA, Zabicki et al. reported that classification accuracies in contralateral M1 during ME were higher than the ones during MI (Zabicki et al., 2017). This suggests that activation patterns in ME to distinguish the right or left were more clearly represented than the pattern in MI because of the different effects of dPMC. As demonstrated in our study, lateralization occurred not only in the neural activity but also in the effective connectivity networks, suggesting that the achievements of ME and MI were largely contralateral, and more information interchange occurred in the contralateral hemisphere.

4.2 Functional gradients in the frontoparietal motor network

We illustrated the direct effects of the frontoparietal motor networks underlying ME and MI tasks (Fig. 3E-H). We found significant positive direct effects from dPMC to SPL and IPS (R-dPMC→R-SPL, L-dPMC→L-SPL, and L-dPMC→L-dIPS) in the same hemisphere across all conditions. This indicates that the direct effects from dPMC to SPL do not depend on modes such as ME and MI. In a previous study that used the conditional GCM, bidirectional effective connectivity between the dPMC and SPL/IPL in the same hemisphere was identified from fMRI data during ME and MI (Gao et al., 2011). In their results, bidirectional effective connectivity represents the forward and backward interactions between the dPMC and SPL during the visual-cued motor task. This suggests that SPL might be associated with the process of somatosensory

modality and visual information and its integration.

We also found negative direct effects (L-vPMC → R-SPL, R-vPMC → L-SPL) across the hemispheres. There are functional similarities and differences in PMC across the dorsal-ventral axis, such as prediction of sequential finger movement (Nambu et al., 2015), representation of chuck of sequential finger movement (Yokoi & Diedrichsen, 2019), encoding spatial location (Gallivan et al., 2011), and linguistic motor planning of fingers (Hanakawa et al., 2005). In the prediction of simple sequential finger movements and the chunking of finger movements, spatial patterns in dPMC and vPMC can be distinguished using MVPA. Thus, simple sequences are commonly represented in these two regions. On the other hand, a specific role of vPMC is to encode target locations depending on head- or eye-centered coordinates and arm/limb-centered coordinates (Gallivan et al., 2011). In a study by Hanakawa et al., neural representations in vPMC mediate the mapping of linguistic stimulus onto the motor planning of fingers (Hanakawa et al., 2005). Owing to motor and nonmotor sequences, activations in vPMC are enhanced during ME and MI tasks. This suggests that functions in vPMC are associated with encoding effectors and spatial coordination.

No studies have evaluated the effective connectivity, including vPMC and SPL (Gao et al., 2011; Kasess et al., 2008). We found that contralateral vPMC negatively affects the ipsilateral SPL. It is suggested that contralateral vPMC

may inhibit brain activity in the ipsilateral SPL. Diedrichsen et al. reported that fMRI signals during ipsilateral finger presses decreased in R-SPL and increased in L-PMC (Diedrichsen et al., 2013). In the case of ipsilateral motor control, only a few regions were able to code sequences and chunks, as reported by Yokoi and Diedrichsen (2019). Neural activity in the SPL during contralateral finger tapping is communicating with dPMC in the same hemisphere for integration of somatosensory and visual processes. To enhance laterality and spatial information, it might be the decoupling of the contralateral vPMC and ipsilateral SPL.

Interestingly, DirectLiNGAM selected direct effects from the frontal to parietal regions, but did not select the effects with opponent direction. This is inconsistent with the results of Gao et al., such as bidirectional effective connection between frontoparietal regions (Gao et al., 2011). Our dSMI task, modulates laterality of hands (right/left) and modes (MI/ME) with finger movement only. The parietal regions are important to encode spatial processing of target or effector-specific coordinates; therefore, neural representation of gestures/actions with hand/foot have been predicted by classification methods, (three right-hand actions: aiming, extension-flexion, and squeezing: (Pilgramm et al., 2016); three right-hand actions and their imagery (Zabicki et al., 2017); touching left/right and gazing left/right (Gallivan et al., 2011)). In these cases, integration of somatosensory and visual processes is important; however, the dSMI task is not required for spatial motor control. Additionally, DirectLiNGAM

does not select redundant direct edges in the optimization process. In future studies, we can explore an estimation of DAG, including the visual cortex, during motor tasks with spatial manipulation, and how the direct effects are represented between frontoparietal networks.

4.3 Audio motor network associated with ME and MI

We found a connection between L-A1 and R-A1 (Fig. 3) and a connection from R-A1 to R-M1 (Fig. 4H). We did not expect to find connections related to A1 when we designed this study because we assumed A1 was a control. Decoding accuracies of modality (ME vs. MI) in A1 were significant in a study by Zabicki et al. (2017). This is consistent with our result using MVPA with a support vector machine in Supplementary Figure 1. There are two different anatomical and functional streams of auditory processing in humans (Jasmin et al., 2019; Lima et al., 2016). Sounds are processed in parallel along two segregated streams, an anteroventral ("what": recognition and identification of auditory objects) stream and a posterodorsal ("where/how": sensorimotor integration and spatial processing) one, both projecting from A1. The anteroventral stream involves the auditory association cortex in the superior temporal gyrus and inferior temporal gyrus. The posterodorsal pathway is along with the posterior temporal fields, IPS, motor and sensory areas, and inferior frontal gyrus. It is important for speech, vocalization, and music to involve auditory and motor areas. Lima et al. reviewed the roles of the SMA and pre-SMA in auditory processing and auditory imagery, and suggested that activating sound-related motor representation in

the SMA and pre-SMA might facilitate behavioral responses to sounds (Lima et al., 2016). On the other hand, Morillon et al. (2015) mentioned that connections between auditory and premotor/motor areas have not been established in primates, and are either weak or absent. Our results indicate that there are direct effects on the audiomotor pathway, in particular, from the contralateral A1 to the contralateral M1 in the same hemisphere. In our task, the participant was instructed to follow the beep sound to tap their finger or image finger tapping. Periodic sound associated with motor control may facilitate the preparation of the next finger movement following the sound sequence.

4.4 Methodological consideration of LiNGAM analysis

The DirectLiNGAM algorithm is a suitable approach to explore the causal relationships between multiple nodes (Shimizu et al., 2011). The conventional method, such as DCM or GCM, has some inherent limitations in treating three or more time series. One main limitation is that if brain regions A and B are both driven by region C but with a different lag, there will be a Granger causality between A and B. To address this problem, the GCM method has been proposed and applied to field potential data from macaque monkeys when performing a GO/NO-GO visual pattern discrimination task and human fMRI data during a face matching task. Afterwards, GCM has improved to apply more than the data of three nodes employing a conditional variable similar to the partial correlation analysis.

In contrast, the DirectLiNGAM algorithm is identifiable by a multivariate dataset of more than three variables. The advantages of this algorithm are as follows: i) a full and unique causal structure can be identified, provided all assumptions hold and the sample size of the observations is sufficiently large. ii) No prior knowledge of the network structure is needed, and iii) compared to DCM, which may involve large numbers of conditional independent tests, the computational complexity of LiNGAM is much lower (Smith et al., 2011). However, DirectLiNGAM is assumed to be DAG and to prune weakly contributed edges with sparseness, therefore, there is a possibility to miss bidirectional effective connectivity. It is necessary to evaluate how the different bidirectional effects are represented in GCM and DirectLiNGAM in future studies.

5. Conclusions

In applying DirectLiNGAM to the fMRI data, we demonstrated that DAG represented the frontoparietal motor network underlying ME and MI. We developed a delayed sequential movement and imagery (dSMI) task extended from Hanakawa et al. (2008) to acquire enough fMRI data samples under ME and MI conditions. We illustrated the frontoparietal motor network with effective connectivity during MI and ME with the right/left hand. Furthermore, we evaluated not only the difference between ME and MI, but also the difference between a dominant-hand and an opposite one to illustrate the asymmetricity of the motor network. Our results demonstrated the inter-regional interactions

among overlapped core regions recruited in ME and MI in the frontoparietal network, including M1, dPMC, vPMC, IPL, SPL, and IPS, thereby, expanding the prior findings of the effective connectivity network on ME and MI. Furthermore, MI not only has kinesthetic aspects, but also auditory aspects, the predominance of which may differentially modulate the participation of the neural substrates in A1. Our approach has the limitations to represent bidirectional interactions and the assumption of independence for each variable. It is necessary to compare several methods how represents causalities of multiple brain regions. Our findings might help to understand interactions across bilateral frontoparietal networks in large-scale underlying ME and MI.

Acknowledgements

This study was supported by JSPS KAKENHI Grant Number JP18H05395, JP18KK0284, the ImPACT Program of the Council for Science, Technology and Innovation (Cabinet Office, Government of Japan), the New Energy and Industrial Technology Development Organization (NEDO), CREST, JST, a contract entitled “Novel and innovative R&D making use of brain structures” with the Ministry of Internal Affairs and Communications, Japan, and the MIC/SCOPE/ #192107002. We thank Manabu Shikauchi and Shigeyuki Ikeda for supporting the MRI experiments, Shohei Shimizu and Aapo Hyvarinen for advising the statistical interpretation of LiNGAM analysis.

Declaration of interest

None

Author contributions

Takeshi Ogawa designed this study and performed data acquisition. Takeshi Ogawa and Hideki Shimobayashi analyzed the data. Takeshi Ogawa, Hideki Shimobayashi, Jun-ichiro Hirayama, and Motoaki Kawanabe discussed data analysis and results. Takeshi Ogawa and Jun-ichiro Hirayama wrote the original draft.

Data and code availability

The data that support the findings of this study are available from the corresponding author, Takeshi Ogawa, upon reasonable request.

References

Apšvalka, D., Cross, E.S., Ramsey, R., 2018. Observing Action Sequences Elicits Sequence-Specific Neural Representations in Frontoparietal Brain regions. *J. Neurosci*. 38, 10114–10128. doi: 10.1523/JNEUROSCI.1597-18.2018.

Brainard, D.H., 1997. The Psychophysics Toolbox. *Spat. Vis. 10*, 433–436. doi: 10.1163/156856897x00357

Deshpande, G., Hu, X., Stilla, R., Sathian, K., 2008. Effective connectivity during haptic perception: a study using Granger causality analysis of functional magnetic resonance imaging data. *Neuroimage*. *40*, 1807–1814. doi: 10.1016/j.neuroimage.2008.01.044.

Destrieux, C., Fischl, B., Dale, A. Halgren, E., 2010. Automatic parcellation of human cortical gyri and sulci using standard anatomical nomenclature. *Neuroimage*. *53*, 1–15. doi: 10.1016/j.neuroimage.2010.06.010.

Diedrichsen, J., Wiestler, T., Krakauer, J.W., 2013. Two distinct ipsilateral cortical representations for individuated finger movements *Cereb. Cortex. 23*, 1362–1377. doi: 10.1093/cercor/bhs120.

Ding, M., Chen, Y., Bressler, S.L., 2006. Granger causality: Basic theory and application to neuroscience in: Schelter, B., Winterhalder, M., Timmer, J. (Eds.), *Handbook of Time Series Analysis: Recent Theoretical Developments and Applications*, *February* 437–460.

Gallivan, J.P., McLean, D.A., Valyear, K.F., Culham, J.C., 2013. Decoding the neural mechanisms of human tool use. *ELife*. *2013*, e00425. doi: 10.7554/eLife.00425

Gallivan, J.P., McLean, D.A., Smith, F.W., Culham, J.C., 2011. Decoding effector-dependent and effector-independent movement intentions from human parieto-

frontal brain activity. *J. Neurosci. 31*, 17149–17168. doi: 10.1523/JNEUROSCI.1058-11.2011.

Gao, Q., Duan, X., Chen, H., 2011. Evaluation of effective connectivity of motor areas during motor imagery and execution using conditional Granger causality. *Neuroimage*. *54*, 1280–1288. doi: 10.1016/j.neuroimage.2010.08.071.

Hanakawa, T. 2016. Organizing motor imageries. *Neurosci. Res. 104*, 56–63. doi: 10.1016/j.neures.2015.11.003.

Hanakawa, T., Dimyan, M.A., Hallett, M., 2008. Motor planning, imagery, and execution in the distributed motor network: A time-course study with functional MRI. *Cereb. Cortex. 18*, 2775–2788. doi: 10.1093/cercor/bhn036.

Hanakawa, T., Parikh, S., Bruno, M.K., Hallett, M., 2005. Finger and face representations in the ipsilateral precentral motor areas in humans. *J. Neurophysiol. 93*, 2950–2958. doi: 10.1152/jn.00784.2004.

Hyvärinen, A., Karhunen, J., Oja, E., 2001. *Independent component analysis.*. Wiley.

Jasmin, K., Lima, C.F., Scott, S.K., 2019. Understanding rostral-caudal auditory cortex contributions to auditory perception. *Nat. Rev. Neurosci. 20*, 425–434. doi: 10.1038/s41583-019-0160-2.

Kasess, C.H., Windischberger, C., Cunnington, R., Lanzenberger, R., Pezawas, L., Moser, E., 2008. The suppressive influence of SMA on M1 in motor imagery revealed by fMRI and dynamic causal modeling. *Neuroimage*. *40*, 828–837. doi: 10.1016/j.neuroimage.2007.11.040.

Kleiner, M., Brainard, D., Pelli, D., Ingling, A., Murray, R., Broussard, C., 2007. *What's new in psychtoolbox-3*. 1–16.

Lima, C.F., Krishnan, S., Scott, S.K., 2016. Roles of Supplementary Motor Areas in Auditory Processing and Auditory Imagery. *Trends. Neurosci*. *39*, 527–542. doi:

10.1016/j.tins.2016.06.003.

Lorey, B., Naumann, T., Pilgramm, S., Petermann, C., Bischoff, M., Zentgraf, K., Stark, R., Vaitl, D., Munzert, J., 2014. Neural simulation of actions: effector- versus action-specific motor maps within the human premotor and posterior parietal area? *Hum. Brain. Mapp*. *35*, 1212–1225. doi: 10.1002/hbm.22246.

Maldjian, J.A., Laurienti, P.J., Kraft, R.A., Burdette, J.H., 2003. An automated method for neuroanatomic and cytoarchitectonic atlas-based interrogation of fMRI data sets. *Neuroimage*. *19*, 1233–1239. doi: 10.1016/s1053-8119(03)00169-1.

Morillon, B., Hackett, T.A., Kajikawa, Y., Schroeder, C.E., 2015. Predictive motor control of sensory dynamics in auditory active sensing. *Curr. Opi. Neurobiol*. *31*, 230–238. doi: 10.1016/j.conb.2014.12.005.

Nambu, I., Hagura, N., Hirose, S., Wada, Y., Kawato, M., & Naito, E., 2015. Decoding sequential finger movements from preparatory activity in higher-order motor regions: a functional magnetic resonance imaging multi-voxel pattern analysis. *Eur. J. Neurosci. 42*, 2851–2859. doi: 10.1111/ejn.13063.

Ogawa, T., Aihara, T., Shimokawa, T., Yamashita, O., 2018. Large-scale brain network associated with creative insight: combined voxel-based morphometry and resting-state functional connectivity analyses. *Sci. Rep. 8*. doi: 10.1038/s41598-018-24981-0.

Oldfield, R.C. 1971. The assessment and analysis of handedness: the Edinburgh inventory. *Neuropsychologia*. 9(1), 97-113. doi: 10.1016/0028-3932(71)90067-4.

Pelli, D.G. 1997. The VideoToolbox software for visual psychophysics: transforming numbers into movies. *Spat. Vis. 10*, 437–442.

Penny, W.D., Stephan, K.E., Mechelli, A., Friston, K.J., 2004. Modelling functional integration: a comparison of structural equation and dynamic causal models.

Neuroimage. *23*, S264–S274. doi: 10.1016/j.neuroimage.2004.07.041.

Pilgramm, S., De Haas, B., Helm, F., Zentgraf, K., Stark, R., Munzert, J., Krüger, B., 2016. Motor imagery of hand actions: Decoding the content of motor imagery from brain activity in frontal and parietal motor areas. *Hum. Brain. Mapp*. *37*, 81–93. doi: 10.1002/hbm.23015.

Rajapakse, J.C., Zhou, J., 2007. Learning effective brain connectivity with dynamic Bayesian networks. *Neuroimage*. *37*, 749–760. doi: 10.1016/j.neuroimage.2007.06.003.

Shimizu, S., Hoyer, P.O., Hyvärinen, A., Kerminen, A. 2006. A Linear Non-Gaussian Acyclic Model for Causal Discovery. *J. Mach. Learn. Res*.*7*, 2003–2030.

Shimizu, S., Inazumi, T., Sogawa, Y., Aapo, H., Takashi, W., Patrik, H. & Kenneth, B. 2011. DirectLiNGAM: A Direct Method for Learning a Linear Non-Gaussian Structural Equation Model. *J. Mach. Learn. Res*.

Smith, S.M., Miller, K.L., Salimi-Khorshidi, G., Webster, M., Beckmann, C.F., Nichols, T.E., Ramsey, J.D., Woolrich, M.W., 2011. Network modelling methods for FMRI. *Neuroimage*. *54*, 875–891. doi: 10.1016/j.neuroimage.2010.08.063.

Xu, L., Fan, T., Wu, X., Chen, K., Guo, X., Zhang, J., Yao, L., 2014. A pooling-LiNGAM algorithm for effective connectivity analysis of fMRI data. *Front. Comput. Neurosci. 8*, 125. doi: 10.3389/fncom.2014.00125.

Yokoi, A., Arbuckle, S.A., Diedrichsen, J., 2018. The Role of Human Primary Motor Cortex in the Production of Skilled Finger Sequences. *J. Neurosci. 38*, 1430–1442. doi: 10.1523/JNEUROSCI.2798-17.2017.

Yokoi, A., Diedrichsen, J., 2019. Neural Organization of Hierarchical Motor Sequence Representations in the Human Neocortex. *Neuron*. *103*, 1178–1190.e7. doi: 10.1016/j.neuron.2019.06.017.

Zabicki, A., De Haas, B., Zentgraf, K., Stark, R., Munzert, J., Krüger, B., 2017. Imagined and Executed Actions in the Human Motor System: Testing Neural Similarity Between Execution and Imagery of Actions with a Multivariate Approach. *Cereb. Cortex. 27*, 4523–4536. doi: 10.1093/cercor/bhw257.

Zhuang, J., LaConte, S., Peltier, S., Zhang, K., Hu, X., 2005. Connectivity exploration with structural equation modeling: An fMRI study of bimanual motor coordination. *Neuroimage*, *25*, 462–470. doi: 10.1016/j.neuroimage.2004.11.007.

Figure captions

Figure 1: Design of the delayed sequential motor imagery and execution (dSMI) task. A participant was asked to remember the instruction stimuli (IS), which were presented for 2 s (1: pointing finger; 2: middle finger; 3: ring finger) and specified a segment of the cue stimuli (CS), which showed conditions, Move, Image, and Listen. According to CS, the participants sequentially tap their fingers (Move), or image to tap (Image), or do nothing (Listen) during D1.

Figure 2: Preprocessing of input data matrix for DirectLiNGAM. (A) An example of a data matrix in single ROI. (B) Time courses of scores of the principle component analysis (PCA) after normalizing the matrix by mean and variance of the matrix for each ROI to decompose loadings and scores. (C) Input data matrix, x, for DirectLiNGAM algorithm. x was collected from only the first principle component (PC1) with sign correction using temporal correlation between the PC1 and a mean time course of the same ROI and concatenated across all subjects for each condition (ME, MI: 18 ROIs × 2,880 samples).
L/R-ME: motor execution with left/right hand; L/R-MI: motor imagery with left/right hand; L/R-FMG: left/right frontomarginal gyrus; L/R-DLPFC: left/right dorsolateral prefrontal cortex; L/R-vPMC: left/right ventral premotor cortex; L/R-dPMC: left/right dorsal premotor cortex; L/R-M1: left/right primary motor cortex; L/R-SPL: left/right superior parietal lobule; L/R-IPS: left/right inferior parietal sulcus; L/R-IPL: left/right inferior parietal lobule; L/R-A1: left/right primary auditory cortex.

Figure 3: Direct acyclic graphs and matrices of effective connectivity estimated by DirectLiNGAM. The direct acyclic graphs show strengths of effective connectivity, B, between two brain regions (A-D), and their color maps of B (E-H). Significant edges were connected between two ROIs (bootstrapping with 1,000 repetitions, $p<0.05$)). Nodes were colored black for frontal motor regions, pink for parietal regions, and green for control regions. A width of the edge shows absolute value of strength of effective connectivity and an arrow of the edge is direction. Positive weights were brightly colored and negative weights were bluely colored. A, E: L-ME; B, F: R-ME; C, G: L-MI; D, H: R-MI. Dotted boxes are covered by d/vPMC-M1 connections (orange), d/vPMC-parietal connections (blue), and audiomotor connections (red) in E, F, G and H.

L/R-ME: motor execution with left/right hand; L/R-MI: motor imagery with left/right hand; L/R-FMG: left/right frontomarginal gyrus; L/R-DLPFC: left/right dorsolateral prefrontal cortex; L/R-vPMC: left/right ventral premotor cortex; L/R-dPMC: left/right dorsal premotor cortex; L/R-M1: left/right primary motor cortex; L/R-SPL: left/right superior parietal lobule; L/R-IPS: left/right inferior parietal sulcus; L/R-IPL: left/right inferior parietal lobule; L/R-A1: left/right primary auditory cortex.

Figure 4: Directed graphs represented differences between two conditions. From two samples estimated from bootstrapping, we illustrated differences of two-sample edges which do not contain 0 within the confidence interval (95%,

two-tails). In (A) L-ME vs L-MI, (B) R-ME vs R-MI, it shows differences between ME and MI. The edges are colored by blue (ME) to red (MI). In (C) R-ME vs L-ME, (D) R-MI vs L-MI, it shows differences between R and L. The edges are colored by blue (ME) to red (MI).

L/R-ME: motor execution with left/right hand; L/R-MI: motor imagery with left/right hand; L/R-FMG: left/right frontomarginal gyrus; L/R-DLPFC: left/right dorsolateral prefrontal cortex; L/R-vPMC: left/right ventral premotor cortex; L/R-dPMC: left/right dorsal premotor cortex; L/R-M1: left/right primary motor cortex; L/R-SPL: left/right superior parietal lobule; L/R-IPS: left/right inferior parietal sulcus; L/R-IPL: left/right inferior parietal lobule; L/R-A1: left/right primary auditory cortex.

Table

Table 1. A list of regional interests applying for the network analysis

#	ROI	Network	#	ROI	Network
1	L-M1	Frontal, motor	10	R-M1	Frontal, motor
2	L-dPMC	Frontal, motor	11	R-dPMC	Frontal, motor
3	L-vPMC	Frontal, motor	12	R-vPMC	Frontal, motor
4	L-SPL	Parietal	13	R-SPL	Parietal
5	L-IPL	Parietal	14	R-IPL	Parietal
6	L-IPS	Parietal	15	R-IPS	Parietal
7	L-A1	Control, auditory	16	R-A1	Control, auditory
8	L-FMG	Control, cognition	17	R-FMG	Control, cognition
9	L-DLPFC	Control, cognition	18	R-DLPFC	Control, cognition

L/R-DLPFC: left/right dorsolateral prefrontal cortex; L/R-vPMC: left/right ventral premotor cortex; L/R-dPMC: left/right dorsal premotor cortex; L/R-M1: left/right primary motor cortex; L/R-SPL: left/right superior parietal lobule; L/R-IPS: left/right inferior parietal sulcus; L/R-IPL: left/right inferior parietal lobule; L/R-A1: left/right primary auditory cortex; ROI: regions of interest

Figure 1

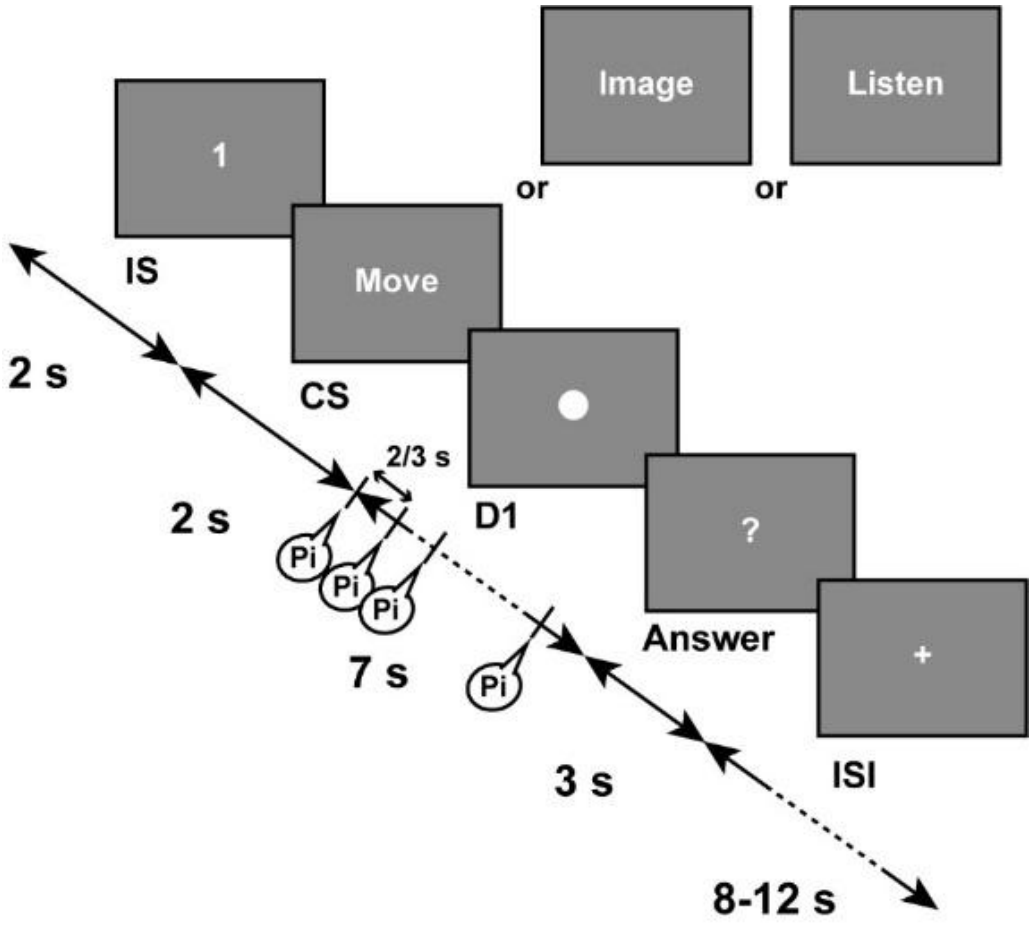
Image
Listen
1
or
or
IS
Move
2 s
CS
2/3 s
2 s
D1
?
Pi
Pi
Pi
Answer
+
7 s
Pi
3 s
ISI
8-12 s

Figure 2

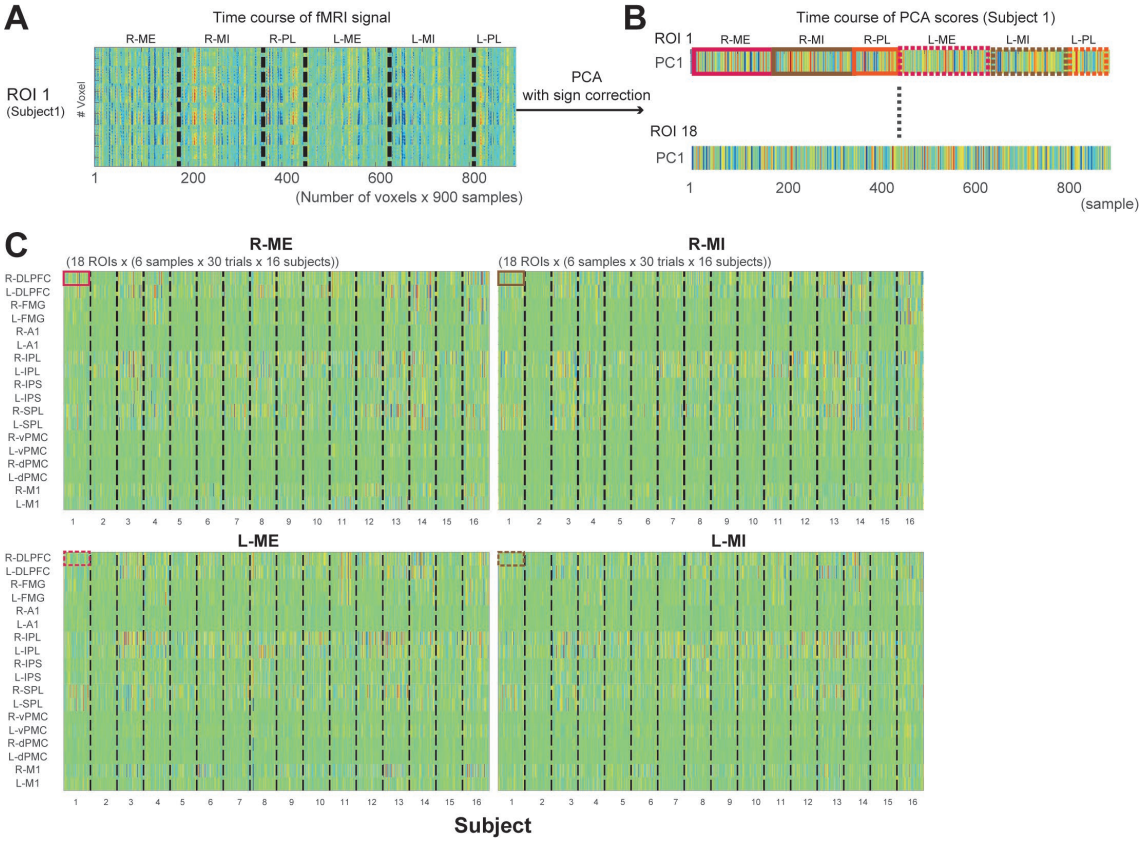
A
Time course of fMRI signal
R-ME
R-MI
R-PL
L-ME
L-MI
L-PL
ROI 1
(Subject1)
Voxel
1
200
400
600
800
(Number of voxels x 900 samples)
PCA
with sign correction
B
Time course of PCA scores (Subject 1)
ROI 1
PC1
ROI 18
(sample)
C
R-ME
(18 ROIs x (6 samples x 30 trials x 16 subjects))
R-MI
L-ME
L-MI
R-DLPFC
L-DLPFC
R-FMG
L-FMG
R-A1
L-A1
R-IPL
L-IPL
R-IPS
L-IPS
R-SPL
L-SPL
R-vPMC
L-vPMC
R-dPMC
L-dPMC
R-M1
L-M1
Subject

Figure 3

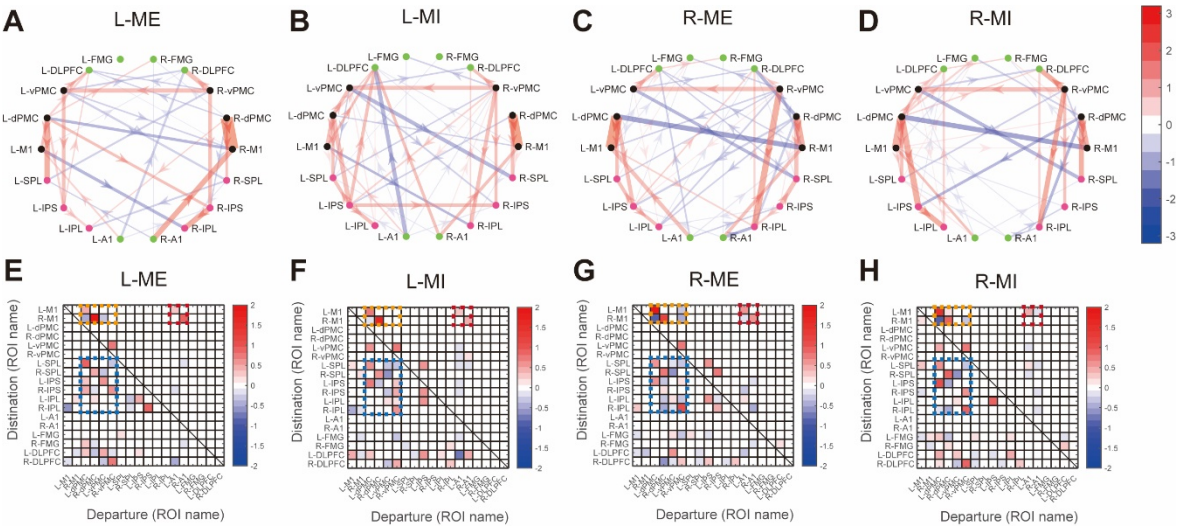
A
L-ME
B
L-MI
C
R-ME
D
R-MI
L-FMG
R-FMG
L-DLPFC
R-DLPFC
L-vPMC
R-vPMC
L-dPMC
R-dPMC
L-M1
R-M1
L-SPL
R-SPL
L-IPS
R-IPS
L-IPL
R-IPL
L-A1
R-A1
E
F
G
H
Distination (ROI name)
Departure (ROI name)

Figure 4

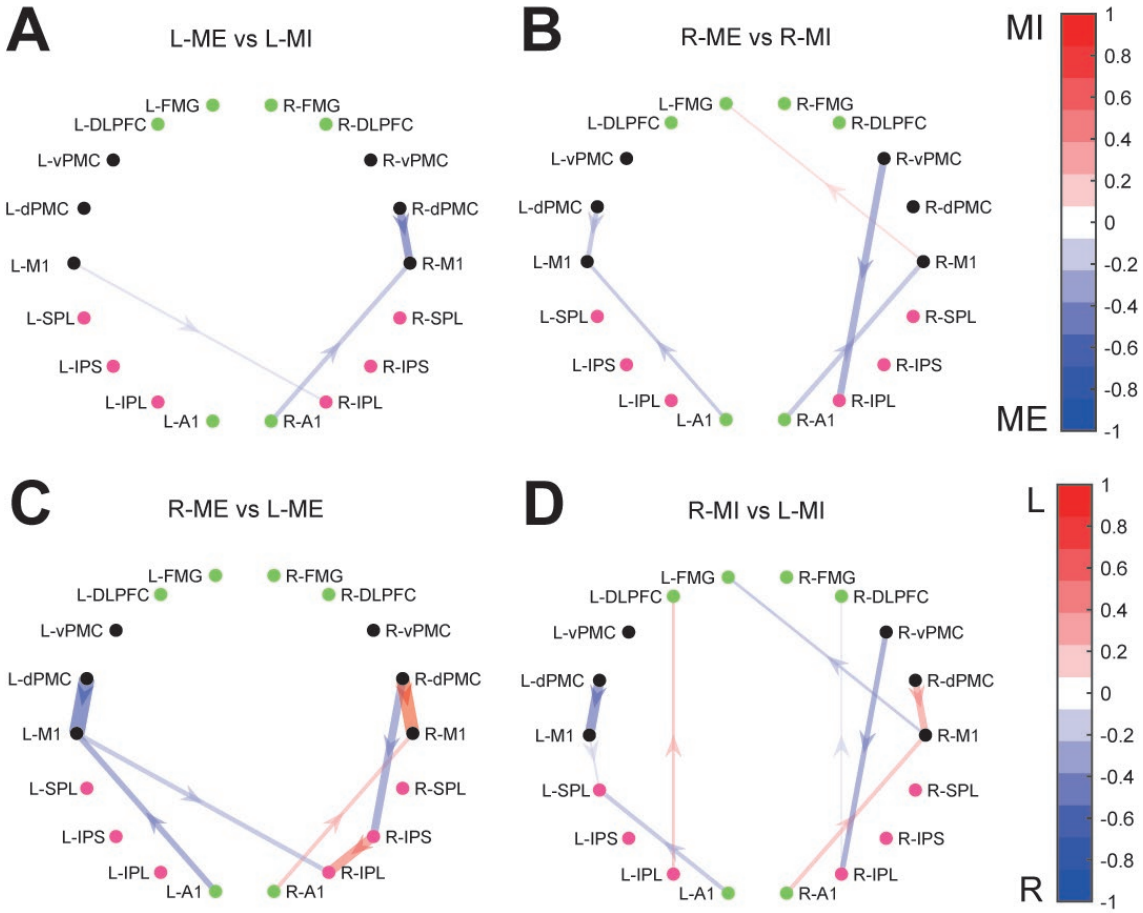
A
L-ME vs L-MI
B
R-ME vs R-MI
C
R-ME vs L-ME
D
R-MI vs L-MI
L-FMG
R-FMG
L-DLPFC
R-DLPFC
L-vPMC
R-vPMC
L-dPMC
R-dPMC
L-M1
R-M1
L-SPL
R-SPL
L-IPS
R-IPS
L-IPL
R-IPL
L-A1
R-A1
MI
ME
L
R
1
0.8
0.6
0.4
0.2
0
-0.2
-0.4
-0.6
-0.8
-1